


Narrow-escape time and sorting of active particles in circular domainsMatteo Paoluzzi ^{*,†} Luca Angelani, and Andrea Puglisi*ISC-CNR, Institute for Complex Systems and Dipartimento di Fisica, Sapienza Università di Roma, Piazzale A. Moro 2, I-00185 Rome, Italy* (Received 16 July 2020; accepted 4 October 2020; published 27 October 2020)

It is now well established that microswimmers can be sorted or segregated fabricating suitable microfluidic devices or using external fields. A natural question is how these techniques can be employed for dividing swimmers of different motility. In this paper, using numerical simulations in the dilute limit, we investigate how motility parameters (time of persistence and velocity) impact the narrow-escape time of active particles from circular domains. We show that the escape time undergoes a crossover between two asymptotic regimes. The control parameters of the crossover is the ratio between the persistence length of the active motion and the typical length scale of the circular domain. We explore the possibility of taking advantage of this finding for sorting active particles by motility parameters.

DOI: [10.1103/PhysRevE.102.042617](https://doi.org/10.1103/PhysRevE.102.042617)**I. INTRODUCTION**

Active particles are widespread in nature [1,2]. Because of their autonomous motion, active particles break fluctuation-dissipation theorem at single-particle level [3] making possible a rich phenomenology that does not share any similarity with equilibrium systems [4–7]. During the last decades, it has been shown that active particles and swimming organisms can be employed for actuating micromotors [8–11], controlling and stabilizing density fluctuations [6,12], or for driving macroscopic directed motion [13,14]. Many aspects of this remarkably phenomenology can be rationalized starting from the morphological properties of the single-particle trajectory. The typical trajectory of an active particle is well captured by a persistent random walk. In particular, the existence of a finite persistence length gives rise to a motion that is ballistic on a short timescale and it becomes diffusive for larger times. It is now well established that, because of the finite persistency, active particles slow down in regions where they are denser [15] and accumulate at the boundaries of a confining container [16–20]. Remarkably, simple artificial environments can be designed for sorting active particles in small regions of space [12]. However, sorting particles dynamically from slower to faster remains a challenge [21]. While some attempts to obtain particles segregation have been made by using external fields [22–24], designing machinery suitable for segregating particles of different motility properties without using any external potential could have important applications, as in the case of *in vitro* fertilization where the identification and gathering of motile sperms without invasive techniques is a hard task [25–28].

In this work, we will focus our attention on the narrow-escape problem of active particles [29–32]. We are interested

in studying this problem numerically in two dimensions considering a circular container with a small target exit site on the boundary. The target site allows particles to escape from the confining structure and we assume that the particles cannot come back into the chamber. Looking at the properties of the first-passage time for a particle to escape from the chamber, we compare two paradigmatic active dynamics, i.e., run-and-tumble and active Brownian. In agreement with recent studies on optimal search strategies with active particles [33], both the active dynamics show a crossover between two regimes in the mean first-passage time. The first regime, typical of active systems, takes place when the persistence length of the random walk is larger than the size of the confining structure. The second regime is reached in the diffusive limit, i.e., when the persistence length is small when compared to the size of the chamber.

Our findings show that, although both dynamics show exactly the same diffusive limit, in the active limit the comparison of different active dynamics at equal persistence times show up differences, with run-and-rumble particles being less efficient than active Brownian in escaping from the chamber. We identify an empirical function $f(x)$ that matches smoothly the two regimes, with $x = \ell/R$, being ℓ the persistence length of the active motion and R the radius of the confining structure. The function captures the crossover between the two scaling regimes that takes place for $x \approx 1$.

Since the two regimes can be reached in either way, by varying the motility parameters or by tuning the size of the confining structure, we show that one can take advantage of the crossover between active and diffusive regime for sorting particles of different persistence length by varying the size of the structure.

II. MODEL AND METHODS

As a model system, we consider a gas of N noninteracting active particles in two spatial dimensions confined to stay inside a circular chamber of radius R . The chamber has a slit of size δ on the boundary where particles can escape (they

^{*}Present address: Departament de Física de la Matèria Condensada, Universitat de Barcelona, C. Martí Franquès 1, 08028 Barcelona, Spain.

[†]matteopaoluzzi@ub.edu

never come back). Indicating with $O = (0, 0)$ the center of the chamber, the slit is displaced symmetrically around $(R, 0)$, i.e., it is represented by the arc included between coordinates $(R \cos \varphi, R \sin \varphi)$ and $(R \cos \varphi, -R \sin \varphi)$, with $\varphi = \delta/2R$. In the present work, we present results for a fixed value of δ . The confining structure is modeled through a repulsive potential $\phi(r) = Ar^{-12}$ [8,34]. The coupling constant A is fixed in a way that a walker pushing against the wall experiences a mechanical force at the boundary such that $f_{\text{self}} = -\phi'|_R$, where the prime indicates the derivative with respect to r , and f_{self} is the self-propulsive force. This mechanical equilibrium condition guarantees that the confining walls are impenetrable. To ensure that the walker, away from the slit, can not displace distances larger than R , the force center of the potential ϕ is located at a finite distance σ beyond the confining wall, i.e., the pointlike walker sees an image particle of radius σ behind the wall [34]. In the following, we express length in unit of $2\sigma = \delta = 1$.

For the active dynamics, we consider two microscopic models: run-and-tumble and active Brownian. Run-and-tumble dynamics has been implemented following Refs. [8,35–37]. Considering the case of overdamped dynamics, that is a good approximation at low Reynolds number, the equation of motion for the particle i is

$$\dot{\mathbf{r}}_i(t) = v_{\text{self}} \hat{\mathbf{e}}_i + \mu \mathbf{f}_{\text{image}}. \quad (1)$$

The versor $\mathbf{e}_i = (\cos \theta_i, \sin \theta_i)$ specifies the swimming direction. $\mu = 1$ is the mobility, $\mathbf{f}_{\text{image}}$ is the short-range force exerted by the image, i.e., $\mathbf{f}_{\text{image}} = -\nabla \phi(r_{\text{image}})$ with $\phi(r) = Ar^{-12}$ [8]. The evolution of $\hat{\mathbf{e}}_i$ depends on the model we consider. In the case of run-and-tumble dynamics [15], $\hat{\mathbf{e}}_i$ stochastically rotates with a rate λ , i.e., the tumbling rate, meaning that a new orientational angle θ is extracted by a uniform distribution in $[0, 2\pi]$ and then it remains constant for a time that is poissonian distributed with rate λ . For active Brownian particles [17], the angle θ_i undergoes the following Langevin dynamics:

$$\dot{\theta}_i(t) = \eta_i, \quad (2)$$

with $\langle \eta_i(t) \rangle = 0$ and $\langle \eta_i(t) \eta_j(s) \rangle = 2D_r \delta_{ij} \delta(t-s)$, with D_r the rotational diffusion constant. Since in experiments with swimming organisms thermal diffusion is orders of magnitude smaller than the diffusion induced by active motion [38,39], in writing Eq. (1) we are neglecting any kind of translational noise.

The tumbling rate λ and the diffusion coefficient D_r fix τ_{pers} that is $\tau_{\text{pers}} = \lambda^{-1}$, and $\tau_{\text{pers}} = D_r^{-1}$, for the two active dynamics, respectively. Using the self-propulsion velocity v_{self} , we can define the persistence length $\ell = v_{\text{self}} \tau_{\text{pers}}$. In both cases, the motion is characterized by a ballistic regime on times $t \ll \tau_{\text{pers}}$ and a diffusive regime for $t \gg \tau_{\text{pers}}$. In two spatial dimensions, the diffusion can be described through the effective diffusion coefficient $D_{\text{eff}} = v_{\text{self}}^2 \tau_{\text{pers}}/2$. We explore a wide range of persistence length by varying motility parameters $\tau_{\text{pers}} \in [10^{-3}, 10]$, $v_{\text{self}} \in [10^{-2}, 10^3]$. The chamber size is changed within the interval $R \in [5, 8 \times 10^2]$.

We solve Eq. (1) numerically integrating the equation of motion using Euler method with a time step Δt ranging from 10^{-3} to 10^{-5} . The numerical integration is performed until each of the runners has reached the target. In the first part of

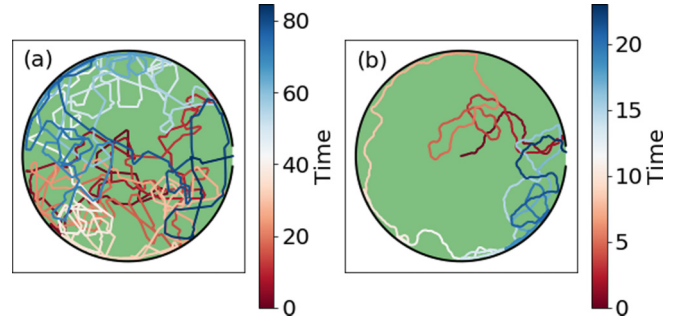


FIG. 1. Active particles escaping from circular domains. A representative trajectory for a single run-and-tumble particle (a) and a single active Brownian particle (b). The parameters are $\lambda = D_r = 1$, $v_{\text{self}} = 1$, $R = 10$. Colors change from red to blue as time increases. In both cases the particle is injected at the center of the chamber and escapes from the circular domain, reaching a slit of width $\delta = 1$ symmetrically displaced around $(R, 0)$.

our work, we consider a gas of noninteracting active particles with same motility parameters v_{self} and τ_{pers} . Particles are injected in the center of the chamber at $t = 0$ and thus the initial density profile $n(\mathbf{r}, 0)$ reads $n(\mathbf{r}, 0) = \frac{N}{\pi R^2} \delta(\mathbf{r})$. We also consider the situation where particles are uniformly distributed at $t = 0$. With both kinds of initial conditions we evaluate the mean first-passage time τ_{FPT} defined as the average time required for escaping from the chamber. τ_{FPT} is computed considering the escape of $N = 10^5$ particles.

In the second part we consider a mixture of particles injected in the center, with motility parameters (v_{self} or τ_{pers}) extracted from a uniform distribution. In this case, we are interested in the evolution of $n(v, t)$ and $n(D_r, t)$ with $n(\cdot, t) \equiv N(\cdot, t)/N(\cdot, 0)$ and $N(\cdot, t)$ the number of particles at time t with a given value of motility parameters.

III. ESCAPE OF A POPULATION WITH IDENTICAL PARAMETERS

The typical trajectories of run-and-tumble and active Brownian dynamics are shown in Fig. 1. Both dynamics share the same motility parameters, i.e., $\lambda = D_r = 1$ and $v_{\text{self}} = 1$. Particles are confined into a circular chamber of radius $R = 10$. As one can see, in either cases, the typical trajectory is a persistent random walk, as it is well known in the literature [1]. Active Brownian dynamics generate smoother trajectories compared with those obtained through run-and-tumble. The latter are characterized by straight run interrupted by tumbling events. Because of the confinement, one expects to observe different dynamical behaviors depending on the characteristic size of the circular chamber. In particular, we define the *active regime* when the radius R is smaller than the persistence length ℓ . We thus identify the opposite situation as the *diffusive regime*, i.e., when $R \gg \ell$.

It is worth noting that a given value of D_{eff} can be obtained through different combinations of v_{self} and τ_{pers} . Moreover, the genuine diffusive limit is recovered performing simultaneously the limit $v_{\text{self}} \rightarrow \infty$ and $\tau_{\text{pers}} \rightarrow 0$ at fixed D_{eff} , as it was realized by Kac in a seminal paper on the telegrapher's equation [40]. As we will see in the next section,

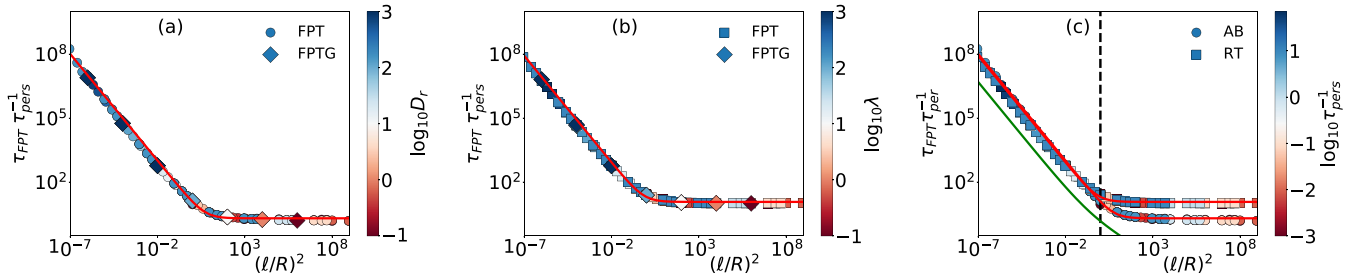


FIG. 2. Mean first-passage time of active walkers escaping from circular domains. τ_{FPT} , in unit of persistence time τ_{pers} (which is $1/\lambda$ or $1/D_r$ for run-and-tumble or active Brownian particles respectively), is reported against the nondimensional parameter ℓ^2/R^2 , for active Brownian (a) and run-and-tumble (b) particles. Diamonds in panels (a) and (b) indicate τ_{FPTG} , in which the initial position is taken with uniform distribution in the chamber. Circles (squares) indicate results with an initial position set at the center of the chamber. (c) Comparison between run-and-tumble and active Brownian dynamics. The persistence length is varied by exploring different motility parameters, i.e., $\tau_{\text{pers}} \in [10^{-3}, 10]$, $v_{\text{self}} \in [10^{-2}, 10^3]$, and also by changing the chamber size, i.e., $R \in [5, 8 \times 10^2]$. The red lines are fit to the empirical function $f(x)$, see text, Eq. (3). The green curve in panel (c) is Eq. (4).

both models show the same diffusive limit that is consistent with the dynamics of a Brownian walker coupled to a thermal bath with effective temperature $k_B T_{\text{eff}} = \mu^{-1} D_{\text{eff}}$, with k_B the Boltzmann constant. To conclude this overview of model parameters, we recall that $2D_{\text{eff}}\tau_{\text{pers}}/R^2 = \ell^2/R^2$, therefore fixing (at given R) τ_{pers} and ℓ also fixes D_{eff} . Most importantly, the condition $R \ll \ell$ ($R \gg \ell$) is equivalent to $D_{\text{eff}}\tau_{\text{pers}} \gg R^2$ ($D_{\text{eff}}\tau_{\text{pers}} \ll R^2$).

The mean first-passage time τ_{FPT} is shown in Fig. 2, rescaled by the persistence time τ_{pers} . Following the previous discussion, as nondimensional control parameter we use $(\ell/R)^2 \equiv 2D_{\text{eff}}\tau_{\text{pers}}/R^2$. Here we are considering a situation where the persistence length is changed by varying both the motility parameters, i.e., the persistence time τ_{pers} , and the self-propulsion velocity v_{self} (therefore different values of D_{eff} are considered). Figure 2(a) refers to active Brownian, and Fig. 2(b) refers to run-and-tumble. We have also varied the radius R of the chamber; see Fig. 2(c).

In the *active regime*, i.e., $\ell \gg R$, τ_{FPT} follows the same asymptotic scaling behavior in both models. However, the fact that run-and-tumble and active Brownian trajectories are *morphologically* different has a quantitative impact on τ_{FPT} away from the diffusive limit. This result is consistent with escape time of active particles from a maze [41].

Figure 2 provides evidence of a collapse of data onto a master curve which is similar but not identical for the two dynamics. In both dynamics $\tau_{\text{FPT}}/\tau_{\text{pers}}$ undergoes a crossover from large values at small persistence length (diffusive regime) to small values at large persistence length (active regime). The color code indicates the inverse of the values of the persistence time τ_{pers} . We have also reported data obtained with a different initial condition (diamonds in figure). In this case, the starting position is uniformly distributed and the results neatly superimpose on the master curve.

On a more quantitative level, we see that the diffusive regime, $\ell \ll R$ ($D_{\text{eff}}\tau_{\text{pers}} \ll R^2$), is signaled by a scaling $\tau_{\text{FPT}}/\tau_{\text{pers}} \sim (\ell/R)^{-2} = R^2/(D_{\text{eff}}\tau_{\text{pers}})$ which implies $\tau_{\text{FPT}} \sim R^2/D_{\text{eff}}$. In the opposite limit, i.e., $\ell \gg R$, where the active regime dominates, we observe a scaling $\tau_{\text{FPT}} \sim \tau_{\text{pers}}$.

In Fig. 2(c) we compare the master curves for the run-and-tumble and active Brownian dynamics. In this case, we are varying only the persistence time τ_{pers} , i.e., the tumbling rate

λ , in the case of run-and-tumble particles, and the rotational diffusion D_r , for active Brownian particles. The *diffusion limit* is thus approached for $\tau_{\text{pers}} \rightarrow 0$, the *active limit* as soon as $\tau_{\text{pers}} \rightarrow \infty$. As one can see, they reach exactly the same diffusive limit when $D_{\text{eff}}R^{-2} \rightarrow 0$. In the opposite limit, i.e., $D_{\text{eff}}R^{-2} \rightarrow \infty$, $\tau_{\text{FPT}} \sim \tau_{\text{pers}}$, however, run-and-tumble particles are systematically slower in finding the exit than active Brownian particles. We can guess that this difference is due to the fact that active Brownian particles, at variance with run-and-tumble, smoothly change their self-propulsion direction.

The behavior observed in the active regime is consistent with optimal research strategies of run-and-tumble in spherical confinement [33]. The divergence of τ_{FPT} with the persistence time can be rationalized noticing that, when $\tau_{\text{pers}} \rightarrow \infty$, only the walkers moving toward the right direction, i.e., with $\theta \in [-\varphi, \varphi]$, can escape from the chamber, therefore the escape becomes more and more difficult. However, analytical predictions of τ_{FPT} for active dynamics remains an open problem [29,30,33,42–44]. For the diffusive regime ($R \gg \ell$) the boundary is so far that active particles displace a distance $\langle \Delta x^2 \rangle = D_{\text{eff}}t$ and thus the boundary is reached on a timescale R^2/D_{eff} , as we observe.

Noticeably, these two asymptotic regimes match smoothly at $\ell R^{-1} = 1$. Indicating with $x = \ell^2 R^{-2}$ the control parameter, we thus propose the following empirical function $f(x)$ that results suitable for capturing the whole emerging phenomenology of the nondimensional quantity $\tau_{\text{FPT}}/\tau_{\text{pers}}$

$$f(x) = \frac{\alpha}{x} + \beta, \quad (3)$$

with α and β which in principle may depend upon R . For instance, in Ref. [33] (where the geometry has important differences with our setup) $\alpha \sim \log(R/\delta)$ and $\beta \sim R/\delta$. Here we find $\alpha = 10.3$ and $\beta = 2.0$ for active Brownian particles and $\alpha = 8.5$ and $\beta = 11.9$ for run-and-tumble particles. Our values of α and β fit data in a wide range of $R \in [5, 8 \times 10^2]$; see Fig. 2. Just for comparison, in the one-dimensional case one has the exact expression for the mean first-passage time [45,46]

$$f_{1d}(x) = 1/2x + 1/\sqrt{x}. \quad (4)$$

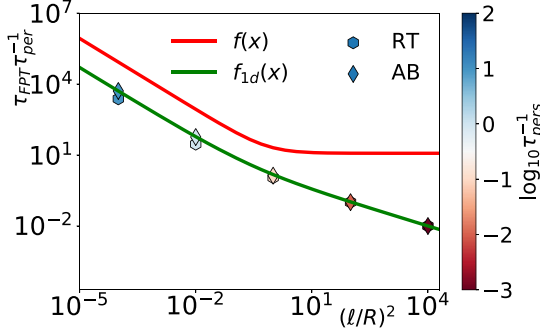


FIG. 3. Mean first-passage time of reaching the boundary; the green curve is Eq. (3), and for comparison we include Eq. (4) as a guide to the eye (red curve).

However, we note that this expression is obtained considering a particle which reaches for the first time the boundary points, corresponding in our two-dimensional case to a particle that escapes once reaching the circular boundary, i.e., $\delta = 2\pi R$. As one can see in Fig. 3, where we computed the escape time for reaching the boundary, $f_{1d}(x)$ reproduces the numerical data. At large persistence lengths ($x \gg 1$) the time to hit the boundary is dominated by the term $\sim 1/\sqrt{x} \sim 1/v_{\text{self}}$, as expected for a purely ballistic motion. This behavior is quite different from that seen at large x in Fig. 2, i.e., for the narrow-escape problem: Curve $f_{1d}(x)$ is plotted in Fig. 2(c) for comparison.

These findings show that particles moving in an environment characterized by a length scale $R > \ell$ are dramatically disadvantaged in finding the exit with respect to particles such that $R < \ell$. As we will show in the next section, this observation can be employed for the purpose of sorting particles with different persistent lengths.

IV. DESIGNING SIMPLE SORTING DEVICES

In this section we explore the possibility of tuning the geometrical properties of the confining structure for sorting particles of different velocities and persistence times. The advantage of this approach relies on the fact that (i) we do not have to introduce any external field, (ii) the geometry is extremely simple and easily realised in microfluidics, as compared to Ref. [12], (iii) the only parameter we have to tune is the radius R . In the following we will show that a device characterized by a given radius $R = 10$ can be employed for sorting active particles of different persistence length ℓ .

According to the results of the previous sections, τ_{FPT} shows a crossover around $R\ell^{-1} = 1$ between two regimes characterized by different scaling laws. To make it explicit, we rewrite here Eq. (3) in terms of the motility parameters for the mean exit time:

$$\tau_{\text{FPT}} = \alpha \frac{R^2}{v_{\text{self}}^2 \tau_{\text{pers}}} + \beta \tau_{\text{pers}}. \quad (5)$$

It is immediately understood that changing v_{self} at constant τ_{pers} leads to a monotone behavior, with a smooth crossover when the two contributions in the right-hand side of Eq. (5) are of the same order, i.e., at $v_{\text{self}} \approx v_{\text{self}}^*$, with $v_{\text{self}}^* = \sqrt{\alpha/\beta R/\tau_{\text{pers}}}$, from a diffusive regime with slow escape to the

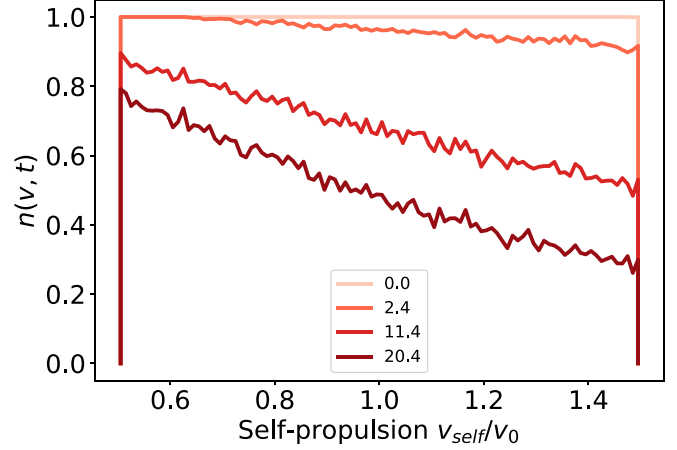


FIG. 4. Mixture of particles with different velocities. Time evolution of $n(v, t)$ at four representative times. In unit of persistence length, the radius of the chamber is $R/\ell = 1$ and rotational diffusion $D_r = 1$. The initial distribution is uniform in the interval $v_{\text{self}}/v_0 \in [0.5, 1.5]$, with $v_0 = 10$.

active regime with fast escape. On the contrary, changing τ_{pers} at constant v_{self} produces a *nonmonotone* behavior with an optimal escape at $\tau_{\text{pers}} \approx \tau_{\text{pers}}^*$, with $\tau_{\text{pers}}^* = \sqrt{\alpha/\beta R}/v_{\text{self}}$ and slower escape both for smaller and larger values of τ_{pers} . In both cases we foresee applications in sorting problems, with different ways of use.

A. Different propulsion velocities

We start by considering a gas composed by particles with different self-propulsion velocity. The velocity is extracted from a uniform distribution. We consider a system composed by $N = 5 \times 10^4$ active Brownian particles in a circular chamber of size $R = 10$ where a small slit of size $\delta = 1$ allows particles to escape. The system is characterized by the initial distribution of self-propulsion velocities $\rho(v) = \frac{1}{v_{\text{max}} - v_{\text{min}}} [\vartheta(v - v_{\text{min}}) - \vartheta(v - v_{\text{max}})]$, with $\vartheta(x)$ the Heaviside step function. Here $v_{\text{max}} = 15$ and $v_{\text{min}} = 5$. All particles have the same rotational diffusion constant $D_r = \tau_{\text{pers}}^{-1} = 1$. In this way, each particle i has its own persistence length $\ell_i = v_{\text{self}}^i$. According to previous results we expect a crossover at $v_{\text{self}}^* \approx 10$: faster particles escape within a time of order 1 on average, slower particles escape in a much slower time, sensitive upon v_{self} .

We are interested in the time evolution of the number of particles with velocity v that falls into the interval $v \in [v, v + dv]$, with $dv = (v_{\text{max}} - v_{\text{min}})/\mathcal{N}$, with $\mathcal{N} = 100$.

In Fig. 4 the time-evolution of $n(v, t)$ is shown as a function of v for four time steps. The distribution is uniform at $t = 0$ and then it changes as soon as particles start to leave the container. As one can see, at a given time $t < t^*$, with $t^* = R/v_{\text{self}}^*$, the only particles escaped are those whose self-propelled velocity satisfies the condition $v_{\text{self}} \geq v_{\text{self}}^*$. With increasing time, also particles with $v_{\text{self}} < v_{\text{self}}^*$ start to escape from the chamber, with times that depend upon v_{self} .

An alternative—and informative—way of seeing these results is studying the relaxation dynamics toward zero of $n(v, t)$ as a function of time. We recall that $n(v, t)$ at a given

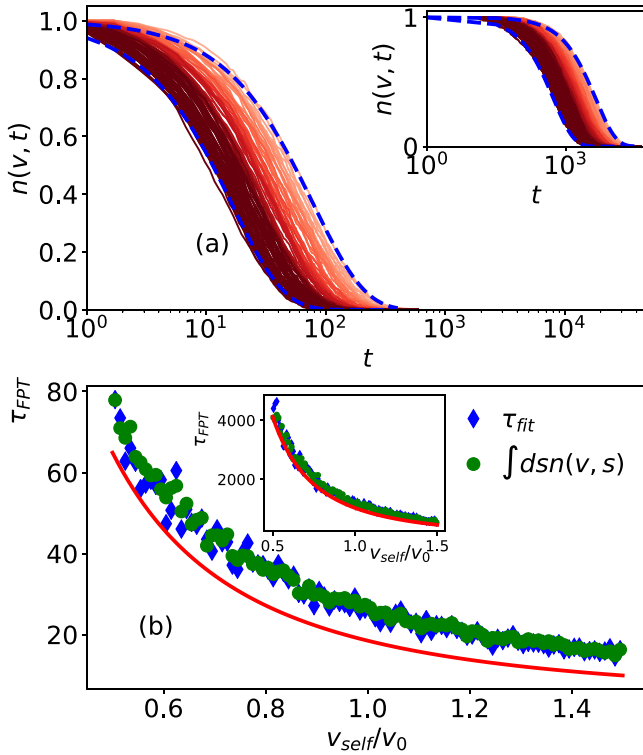


FIG. 5. Decay of the number density for different v_{self} . (a) Time evolution of $n(v, t)$ for the different velocity components v_{self} , the velocity decreases from 10 (dark red) to 5 (light red). The decay of $n(v, t)$ is well captured by an exponential curve (dashed blue lines are fit with $n_{\text{fit}}(v, t) = Ae^{-t/\tau(v)}$). Inset: same observable for $R = 10$ and $v_{\text{self}} \in [0.5, 1.0]$. (b) The exit time $\tau(v)$ computed by fitting $n(v, t)$ to an exponential decay (blue diamonds) and using Eq. (8) with $R = 10$ and $v_{\text{self}} \in [5, 10]$ [Inset: $v_{\text{self}} \in [0.5, 1.0]$]. Solid red curve is the empirical function $f(x)$ Eq. (3).

$v = v_{\text{self}}$ is the survival probability in this problem, which is the complementary cumulative of the probability density function $p(v, s)$ of having first exit at time s :

$$n(v, t) = \int_t^\infty dsp(v, s), \quad (6)$$

or equivalently

$$p(v, s) = -\frac{dn(v, t)}{dt}. \quad (7)$$

The results are reported in Fig. 5. In Fig. 5(a), $n(v, t)$ is shown for different values of self-propulsion velocities, increasing from light to dark red. We notice that a simple exponential relaxation characterized by a single velocity-dependent timescale $\tau(v)$ might capture the behavior of $n(v, t)$ as a function of time. We show the results of exponential fits of the decay $n_{\text{fit}}(v, t) = A \exp[-t/\tau_{\text{fit}}(v)]$, with $A \sim 1$. Dashed blue curve in Fig. 5(a) are two representative fits for $v_{\text{min}} = 5$ and $v_{\text{max}} = 15$. In the inset of Fig. 5(a), we show the decay of $n(v, t)$ for self-propulsion velocity uniformly distributed around $v_{\text{min}} = 0.5$ and $v_{\text{max}} = 1.5$, i.e., velocities much smaller than the threshold velocity $v_{\text{self}}^* \approx 10$.

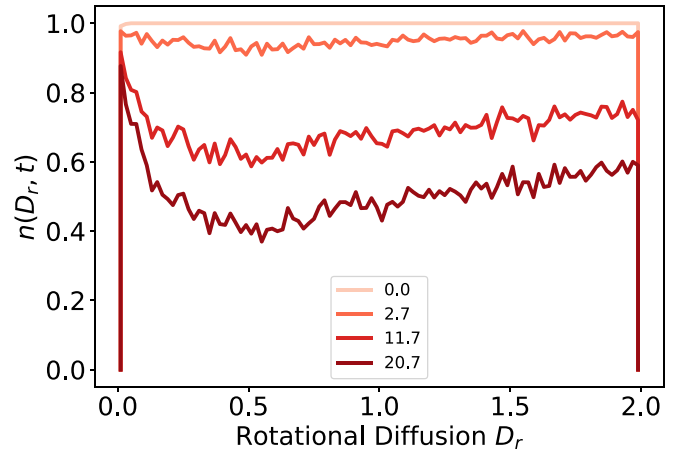


FIG. 6. Mixture of particles with different persistence times. Time evolution of $n(D_r, t)$ at six representative times. In unit of persistence length, the radius of the chamber is $R/\ell = 1$. The initial distribution $n(D_r, 0)$ is uniform in the interval $D_r \in [0, 2]$.

Moreover, in view of Eq. (7), the knowledge of $n(v, t)$ gives us immediate access to the average mean first exit time:

$$\begin{aligned} \tau_{\text{FPT}}(v) &= \int_0^\infty ds sp(v, s) = - \int_0^\infty ds s \frac{dn(v, s)}{ds} \\ &= \int_0^\infty ds n(v, s). \end{aligned} \quad (8)$$

It is worth noting that, in the case of a purely exponential relaxation, i.e., $n(v, t) = e^{-t/\tau_{\text{fit}}(v)}$, $\tau_{\text{FPT}}(v)$ coincides with τ_{fit} . The behavior of τ_{FPT} as a function of v_{self} is shown in Fig. 5(b). As one can appreciate, τ_{FPT} and τ_{fit} are in a nice agreement for $R = 10$ and $v \in [5, 10]$. The solid curve is Eq. (5) with the values of the parameters α and β previously fitted. In the main plot, the crossover can be appreciated from small to large velocities where τ_{fit} decays and then starts to follow the $1/v_{\text{self}}^2$ scaling for small velocities. When $R = 10$ and $v_{\text{self}} \in [0.5, 1.5]$, on the contrary, the behavior of τ_{FPT} is dominated by the $1/v_{\text{self}}^2$; see Eq. (5).

B. Different persistence times

In this section we tune the persistence length ℓ by varying the persistence time τ_{pers} —which is $1/D_r$ for the case considered here of active Brownian particles—and maintaining fixed the self-propulsion velocity v_{self} . We investigate the behavior of a sample composed by the same number of particles of the previous case with same self-propulsion velocity, i.e., $v_{\text{self}} = 10$, and characterized by an initial distribution of rotational diffusion $\rho(D_r) = \frac{1}{D_{r,\text{max}} - D_{r,\text{min}}} [\vartheta(D_r - D_{r,\text{min}}) - \vartheta(D_r - D_{r,\text{max}})]$, with $D_{r,\text{max}} = 2$ and $D_{r,\text{min}} = 0$. The results are shown in Fig. 6. Note that, in this case, particles with $D_r = 0$ remain trapped unless they starts with the right direction.

In Fig. 7 the typical behavior of $n(D_r, t)$ as a function of time is shown. In this case we observe for the very low values of D_r (high activity) that a single exponential decay does not reproduce the decay of $n(D_r, t)$.

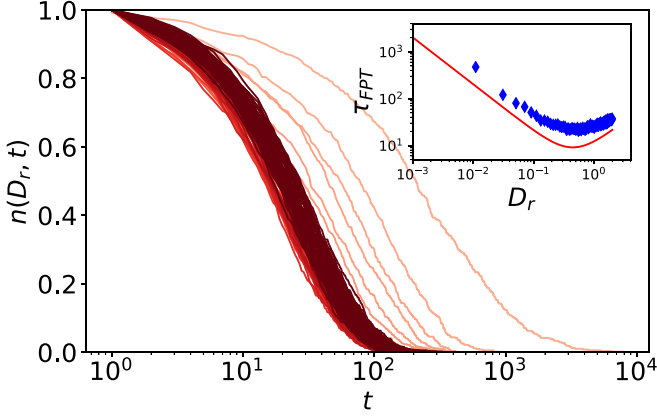


FIG. 7. Decay of the number density for different D_r . Time evolution of $n(D_r, t)$, the rotational diffusion D_r decreases from 2 (dark red) to 0 (light red). Inset: the exit time as a function of D_r . Solid red curve is $f(x)$ with α and β previously fitted from τ_{FPT} .

Again we measure τ_{FPT} from Eq. (8) and plot it in the inset of Fig. 7. According with the scaling of τ_{FPT} we discussed in Sec. III, τ_{FPT} matches two asymptotic regimes, the first one, for small D_r values and thus large persistence length, is $\tau_{\text{FPT}} \sim D_r^{-1}$. The second one is typical of the diffusive regime, meaning that $\tau_{\text{FPT}} \sim D_r$. In the inset of the same figure we report τ_{FPT} as a function of D_r , with superimposed Eq. (5).

C. Behavior of run-and-tumble particles

While the results in the previous sections have been obtained for active Brownian particles, we have performed the same numerical simulations in the case of run-and-tumble dynamics, again for mixtures of particles with different propulsion velocities $v_{\text{self}} \in [5, 15]$, $R = 10$, and persistence times $\tau_{\text{pers}} = 1/\lambda$ with $\lambda \in [0.01, 2]$. The results, shown in Figs. 8(a) and 8(b), respectively, are qualitatively the same of the previous cases: The relaxation dynamics of $n(v, t)$ and $n(\lambda, t)$ are well described by an exponential decay, unless the persistence time is very large ($\lambda \ll 1$). We notice that the nonexponential decay occurs for a larger range of persistence time with respect to the active Brownian case. In our opinion this observation corroborates a correlation between the *nonexponential* decay and ballistic behavior, which suggests that typical exit trajectories at large τ_{pers} are composed of two separate processes: first, the particles reach the boundary and second the particles finds the exit remaining close to the boundary. The behavior of τ_{FPT} is also reported in the insets of the two plots in Fig. 8.

V. DISCUSSION AND CONCLUSIONS

In this work we have proposed a numerical study of the narrow-escape problem of active particles in circular domains. We compared two paradigmatic models of active motions that are active Brownian dynamics [47], suitable for reproducing the trajectories of smooth swimmers, and run-and-tumble dynamics, that, for instance, well captures the morphological properties of *Escherichia coli* trajectories [48]. We showed that in both dynamics τ_{FPT} turns to be bounded by two limiting asymptotic regimes. The two regimes result from the compe-

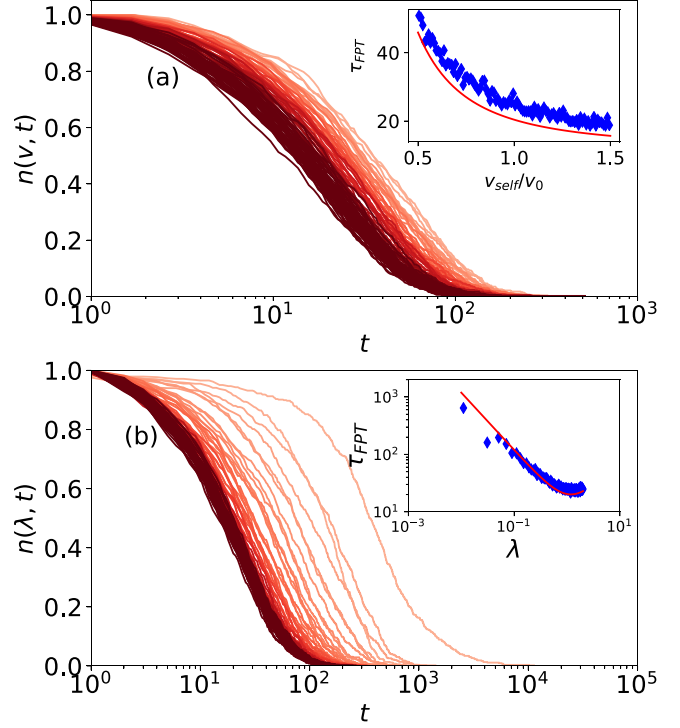


FIG. 8. Sorting of run-and-tumble particles. (a) Time evolution of $n(v, t)$ as a function of t with $v \in [5, 10]$ and $R = 10$. Inset: τ as a function of v_{self} . The dashed red curve is $f(x)$. (b) Time evolution of $n(\lambda, t)$ as a function of t with $\lambda \in [0, 2]$, $v_{\text{self}} = 10$, and $R = 10$. Inset: τ as a function λ .

tion between the two characteristic length scales of the system: the persistence length ℓ and the radius R of the container. When the persistence length is much smaller than the radius, i.e., $\ell/R \ll 1$, the active particles behaves as a Brownian random walker and τ_{FPT} diverges as the effective diffusivity of the random walk goes to zero. In the opposite limit, the persistence length is much larger than the size of the chamber, i.e., $\ell/R \gg 1$. The escaping dynamics is thus dominated by the ballistic regime and τ_{FPT} grows linearly with τ_{pers} . We have introduced an empirical scaling function $f(x)$, with $x = \ell^2 R^{-2}$, that smoothly connects these two asymptotic regimes.

We thus explored the possibility to take advantage of the crossover in the escape time between the active and the diffusive regime for sorting particles of different velocities. We obtained that, considering a gas of active Brownian particles of different velocities and same rotational diffusion constant, by tuning the size of the chamber faster particles can be separated by the others. The same technique can be employed for demixing particles of different rotational diffusion. We showed that the same is true also in the case of run-and-tumble dynamics.

In this study, we have not considered mechanical interactions between particles. Mechanical interactions can be seen as an extra source of collisions and thus, at least for small densities, they renormalize the tumbling-rate λ (the rotational diffusion D_r in the case of active Brownian particles). As shown in Ref. [36], λ becomes a density-dependent function. In particular, $\lambda(\rho)$ increases as density increases, i.e., $\lambda(\rho) = \lambda + A\rho + o(\rho^2)$, with $A > 0$. If this were the only

effect, one can expect that in the dilute regime mechanical interactions make the system more diffusive, i.e., the persistence length decreases. This effect can remove the divergency in τ_{EPT} for $\lambda \rightarrow 0$ ($D_r \rightarrow 0$). Moreover, we can speculate that thermal noise might contribute to remove such divergence as well. However, if the persistence length is long enough, then the system will undergo a motility-induced phase separation (MIPS) [49], which happens at moderate densities, and it is not clear how a spinodal decomposition impacts the escape time. Moreover, since particles can leave the chamber, density is a decreasing function of time. The competition between these mechanisms makes it hard to provide predictions without extensive numerical simulations which will be considered in future investigations.

It is worth noting that the sorting mechanism explored here is dynamical and it works only on a finite timescale. In particular, waiting a sufficiently long time, all particles

escape from the confining structure. However, in a practical situation, the typical experimental timescale can be tuned for sorting microswimmers of different velocities tuning just the typical size of the confining structures, i.e., without introducing any external potential or complicated microstructure. This could be useful in assistant reproductive technologies, where the challenge consists in maximizing motile sperm concentration, sperm volume, and lifetime. Usually, sperms are selected based on their motility. Our findings suggest that it could be done without introducing density gradient centrifugation [25,26].

ACKNOWLEDGMENTS

The research leading to these results has received funding from Regione Lazio, Grant No. 85-2017-15257 (“Progetti di Gruppi di Ricerca-Legge 13/2008-art.4”).

-
- [1] C. Bechinger, R. Di Leonardo, H. Löwen, C. Reichhardt, G. Volpe, and G. Volpe, *Rev. Mod. Phys.* **88**, 045006 (2016).
 - [2] M. C. Marchetti, J. F. Joanny, S. Ramaswamy, T. B. Liverpool, J. Prost, M. Rao, and R. A. Simha, *Rev. Mod. Phys.* **85**, 1143 (2013).
 - [3] C. Maggi, M. Paoluzzi, L. Angelani, and R. Di Leonardo, *Sci. Rep.* **7**, 17588 (2017).
 - [4] H.-P. Zhang, A. Be'er, E.-L. Florin, and H. L. Swinney, *Proc. Natl. Acad. Sci. USA* **107**, 13626 (2010).
 - [5] E. Lushi, H. Wioland, and R. E. Goldstein, *Proc. Natl. Acad. Sci. USA* **111**, 9733 (2014).
 - [6] A. Bricard, J.-B. Caussin, N. Desreumaux, O. Dauchot, and D. Bartolo, *Nature* **503**, 95 (2013).
 - [7] T. Sanchez, D. T. Chen, S. J. DeCamp, M. Heymann, and Z. Dogic, *Nature* **491**, 431 (2012).
 - [8] L. Angelani, R. Di Leonardo, and G. Ruocco, *Phys. Rev. Lett.* **102**, 048104 (2009).
 - [9] R. Di Leonardo, L. Angelani, D. Dell’Arciprete, G. Ruocco, V. Iebba, S. Schippa, M. Conte, F. Mecarini, F. De Angelis, and E. Di Fabrizio, *Proc. Natl. Acad. Sci. USA* **107**, 9541 (2010).
 - [10] A. Sokolov, M. M. Apodaca, B. A. Grzybowski, and I. S. Aranson, *Proc. Natl. Acad. Sci. USA* **107**, 969 (2010).
 - [11] C. Maggi, J. Simmchen, F. Saglimbeni, J. Katuri, M. Dipalo, F. De Angelis, S. Sanchez, and R. Di Leonardo, *Small* **12**, 446 (2016).
 - [12] P. Galajda, J. Keymer, P. Chaikin, and R. Austin, *J. Bacteriol.* **189**, 8704 (2007).
 - [13] L. Angelani, A. Costanzo, and R. Di Leonardo, *Europhys. Lett.* **96**, 68002 (2011).
 - [14] C. O. Reichhardt and C. Reichhardt, *Annu. Rev. Condens. Matter Phys.* **8**, 51 (2017).
 - [15] M. J. Schnitzer, *Phys. Rev. E* **48**, 2553 (1993).
 - [16] I. D. Vladescu, E. J. Marsden, J. Schwarz-Linek, V. A. Martinez, J. Arlt, A. N. Morozov, D. Marenduzzo, M. E. Cates, and W. C. K. Poon, *Phys. Rev. Lett.* **113**, 268101 (2014).
 - [17] S. Das, G. Gompper, and R. G. Winkler, *New J. Phys.* **20**, 015001 (2018).
 - [18] L. Caprini and U. M. B. Marconi, *Soft Matter* **14**, 9044 (2018).
 - [19] L. Caprini and U. M. B. Marconi, *Soft Matter* **15**, 2627 (2019).
 - [20] L. Angelani, *J. Phys. A: Math. Theor.* **50**, 325601 (2017).
 - [21] M. Mijalkov and G. Volpe, *Soft Matter* **9**, 6376 (2013).
 - [22] A. Kaiser, H. H. Wensink, and H. Löwen, *Phys. Rev. Lett.* **108**, 268307 (2012).
 - [23] A. Costanzo, J. Elgeti, T. Auth, G. Gompper, and M. Ripoll, *Europhys. Lett.* **107**, 36003 (2014).
 - [24] N. Kumar, R. K. Gupta, H. Soni, S. Ramaswamy, and A. K. Sood, *Phys. Rev. E* **99**, 032605 (2019).
 - [25] R. Nosrati, P. J. Graham, B. Zhang, J. Riordon, A. Lagunov, T. G. Hannam, C. Escobedo, K. Jarvi, and D. Sinton, *Nat. Rev. Urology* **14**, 707 (2017).
 - [26] J. B. Y. Koh *et al.*, *Microfluidics Nanofluidics* **18**, 755 (2015).
 - [27] E. A. Gaffney, H. Gadêlha, D. Smith, J. Blake, and J. Kirkman-Brown, *Annu. Rev. Fluid Mech.* **43**, 501 (2011).
 - [28] A. Campana, D. Sakkas, A. Stalberg, P. G. Bianchi, I. Comte, T. Pache, and D. Walker, *Human Reprod.* **11**, 732 (1996).
 - [29] O. Bénichou and R. Voituriez, *Phys. Rep.* **539**, 225 (2014).
 - [30] A. Singer, Z. Schuss, and D. Holcman, *J. Stat. Phys.* **122**, 465 (2006).
 - [31] S. Chakia and R. Chakrabarti, *Soft Matter* **16**, 7103 (2020).
 - [32] K. S. Olsen, L. Angheluta, and E. G. Flekkøy, [arXiv:2007.08833](https://arxiv.org/abs/2007.08833).
 - [33] J. F. Rupprecht, O. Bénichou, and R. Voituriez, *Phys. Rev. E* **94**, 012117 (2016).
 - [34] M. Paoluzzi, R. Di Leonardo, and L. Angelani, *Phys. Rev. Lett.* **115**, 188303 (2015).
 - [35] M. Paoluzzi, R. Di Leonardo, and L. Angelani, *J. Phys.: Condens. Matter* **26**, 375101 (2014).
 - [36] M. Paoluzzi, R. Di Leonardo, and L. Angelani, *J. Phys.: Condens. Matter* **25**, 415102 (2013).
 - [37] M. Paoluzzi, M. Leoni, and M. C. Marchetti, *Phys. Rev. E* **98**, 052603 (2018).
 - [38] X.-L. Wu and A. Libchaber, *Phys. Rev. Lett.* **84**, 3017 (2000).
 - [39] N. Koumakis, A. Lepore, C. Maggi, and R. Di Leonardo, *Nat. Commun.* **4**, 2588 (2013).
 - [40] M. Kac, *Rocky Mount. J. Math.* **4**, 497 (1974).
 - [41] M. Khatami, K. Wolff, O. Pohl, M. R. Ejtehadi, and H. Stark, *Sci. Rep.* **6**, 37670 (2016).

- [42] S. Redner, *A Guide to First-passage Processes* (Cambridge University Press, Cambridge, UK, 2001).
- [43] A. Singer, Z. Schuss, D. Holcman, and R. S. Eisenberg, *J. Stat. Phys.* **122**, 437 (2006).
- [44] J.-F. Rupprecht, O. Bénichou, D. Grebenkov, and R. Voituriez, *J. Stat. Phys.* **158**, 192 (2015).
- [45] L. Angelani, R. Di Leonardo, and M. Paoluzzi, *Eur. Phys. J. E* **37**, 59 (2014).
- [46] L. Angelani, *J. Phys. A: Math. Theor.* **48**, 495003 (2015).
- [47] J. Bialké, T. Speck, and H. Löwen, *J. Non-Cryst. Solids* **407**, 367 (2015).
- [48] H. C. Berg, *E. coli in Motion* (Springer Science & Business Media, Berlin, 2008).
- [49] M. E. Cates and J. Tailleur, *Annu. Rev. Condens. Matter Phys.* **6**, 219 (2015).